JACS
JOURNAL OF THE AMERICAN CHEMICAL SOCIETY

ARTICLE

pubs.acs.org/JACS

Molecular Explanation for Why Talc Surfaces Can Be Both Hydrophilic and Hydrophobic

Benjamin Rotenberg,*[,†] Amish J. Patel,[‡] and David Chandler[§]

[†]Laboratoire PECSA, UMR 7195, CNRS et UPMC-Paris 6, 4 pl. Jussieu, F-75005 Paris, France

[‡]Howard P. Isermann Department of Chemical & Biological Engineering and Center for Biotechnology and Interdisciplinary Studies, Rensselaer Polytechnic Institute, Troy, New York 12180, United States

[§]Department of Chemistry, University of California, Berkeley, California 94720, United States

Supporting Information

ABSTRACT: While individual water molecules adsorb strongly on a talc surface (hydrophilic behavior), a droplet of water beads up on the same surface (hydrophobic behavior). To rationalize this dichotomy, we investigated the influence of the microscopic structure of the surface and the strength of adhesive (surface−water) interactions on surface hydrophobicity. We have shown that at low relative humidity, the competition between adhesion and the favorable entropy of being in the vapor phase determines the surface coverage. However, at saturation, it is the competition between adhesion and cohesion (water−water interactions) that determines the surface hydrophobicity. The adhesive interactions in talc are strong enough to overcome the unfavorable entropy, and water adsorbs strongly on talc surfaces. However, they are too weak to overcome the cohesive interactions, and water thus beads up on talc surfaces. Surprisingly, even talc-like surfaces that are highly adhesive do not fully wet at saturation. Instead, a water droplet forms on top of a strongly adsorbed monolayer of water. Our results imply that the interior of hydrophobic zeolites suspended in water may contain adsorbed water molecules at pressures much lower than the intrusion pressure.

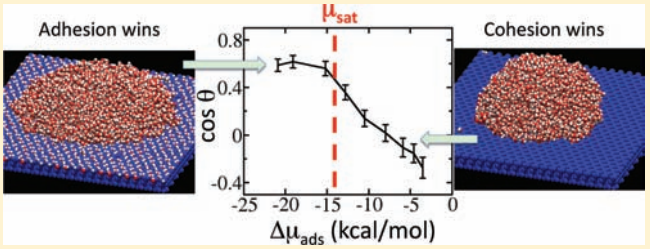

INTRODUCTION

The wetting properties of minerals in soils and rocks play a crucial role in the transport, and thus availability, of water and oil. Clay minerals are particularly interesting not only because of their abundance in nature and synthetic materials but also because the existence of clays with different structures allows us to investigate the effect of surface microstructure on macroscopic properties. Clay surfaces can either be charge-neutral or have a net charge that is balanced by counterions in solution. Molecular simulations have furthered our understanding of both of these types of clays: uncharged clays have been studied using both ab initio[1,2] and classical simulations,[3,4] whereas simulations of charged clays have provided insights into interlayer properties,[5−8] swelling,[9−12] and cation exchange.[13−15] These studies have shown that the surface microstructure is expected to be more important in determining surface−water interactions in uncharged clays,[16,17] and it is these surfaces that are the focus of the present work. Among uncharged clays, talc surfaces have attracted a lot of attention[18−21] because of their peculiar behavior with respect to water. While chemically different surfaces of the same clay mineral (e.g. kaolinite) may display different affinities for water,[22,23] the fact that the same talc surface appears as either hydrophilic or hydrophobic depending on the relative humidity (RH) is rather surprising. Water adsorption at low RH indeed reveals the presence of strong binding sites on talc.[24] Such strong binding sites are absent in similar uncharged clays such as pyrophyllite and fluorotalc. However, experimental contact angles indicate that the surface of talc monocrystals is hydrophobic, similar to that of pyrophyllite.[25,26]

To investigate this dichotomy, we have employed molecular dynamics simulations combined with recently developed algorithms.[27,28] In agreement with experiments, we have found that at low RH, talc surfaces display hydrophilic behavior as water adsorbs strongly to the binding sites on the surface. However, at saturation, cohesive interactions dominate, and the interaction between the surface binding sites and water is minimal, resulting in a hydrophobic surface.

To explore further the role of surface microstructure and the strength of the adhesive interactions on surface hydrophobicity, we have also studied similar clay minerals (pyrophyllite and fluorotalc) as well as modified talc surfaces with a range of binding site polarities at both low relative humidity and saturation. We have found that the dual hydrophilic−hydrophobic behavior observed in talc is generically expected to be manifested for surfaces whose adhesive interaction energy lies in a special range. If the adhesion to water is strong enough to overcome the entropy of being in the vapor phase at low RH, water adsorbs

Received: September 18, 2011
Published: October 28, 2011

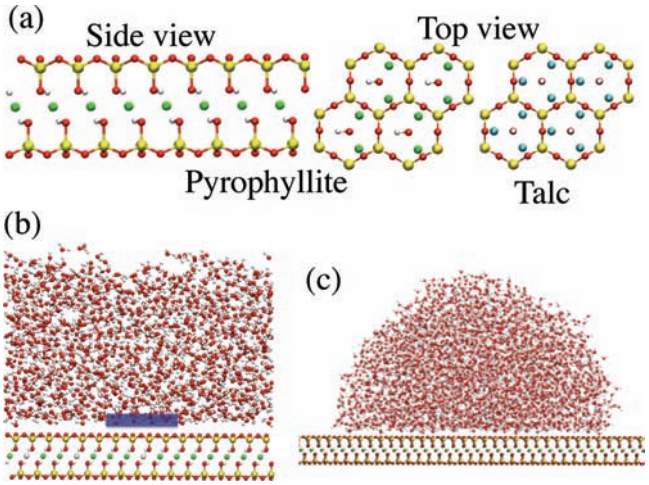

Figure 1. (a) Microscopic clay structures (red, O; white, H; yellow, Si; green, Al; cyan, Mg). The side and top views of the pyrophyllite clay sheet show the hydroxyl (−OH) groups, which are parallel to the sheet. In talc (top view shown), the −OH groups are perpendicular to the sheet and can participate in hydrogen bonding with water. In fluorotalc (not shown), the talc −OH groups are replaced by F atoms. (b) Part of the simulation setup for studying the clay−water interface. The blue box is the observation volume, v, used to probe density fluctuations. (c) Simulation setup for determining contact angles.

strongly to the surface (hydrophilic behavior). At the same time, if adhesion is too weak to overcome the cohesive interactions in water, the surface is hydrophobic at saturation. For modified talc surfaces with strong enough adhesion to overcome the cohesive interactions, all of the surface binding sites are occupied by water molecules at saturation, as expected. Surprisingly, instead of observing complete wetting, we have found that a water droplet sits atop the adsorbed water monolayer.

METHODS

Microscopic Models. Talc, fluorotalc, and pyrophyllite are uncharged clay minerals (i.e., layered silicates of Mg or Al) that belong to the family of TOT clays: each clay sheet consists of a layer of octahedrally coordinated magnesium or aluminum oxide between two layers of tetrahedral silicon oxide (see the side view in Figure 1a). The surfaces of these sheets display hexagonal rings of SiO_2 tetrahedra. In talc and fluorotalc, all of the octahedral sites are occupied by Mg atoms, while in pyrophyllite, two-thirds of these sites are occupied by Al atoms (see the top views in Figure 1a). The charges on Mg and Al are balanced by hydroxyl groups in the center of the hexagonal cavities. In talc, these hydroxyl groups are oriented perpendicular to the surface and can participate in hydrogen bonding with water. In pyrophyllite, the hydroxyl groups are oriented parallel to the surface, and in fluorotalc, they are replaced by fluorine atoms. The atomic coordinates for the unit cells of these clays have been included as Supporting Information.

We used the CLAYFF force field[3] to model the interactions of the clay atoms and the SPC/E model to describe water.[29] Lorentz−Berthelot combination rules were used to determine the pair Lennard-Jones parameters, and a rigid clay structure was assumed. As there are no parameters for fluorine in CLAYFF, we assigned it a charge equal to that of the −OH group in talc (−0.525) and Lennard-Jones parameters of the fluoride ion reported in ref 30. All simulations were performed in the NVT ensemble using the LAMMPS simulation package[31] at T = 300 K, maintained using a Nose−Hoover thermostat.[32] SHAKE was used to integrate the motion of the rigid water molecules,[33] and long-range electrostatic interactions were computed by Ewald summation.

Clay−Water Interface. A clay−water interface is representative of the situation at saturation. The setup shown in Figure 1b was used to calculate the local water density, $\rho(z)$, and the water density fluctuations near the interface. $\mathcal{A}(z)$, the potential of mean force (PMF) for bringing a water molecule from the bulk to a distance z from the plane of the Mg (talc and fluorotalc) or Al (pyrophyllite) atoms is related to $\rho(z)$ by the expression $\mathcal{A}(z) = -k_BT \ln[\rho(z)/\rho_b]$, where k_B is the Boltzmann constant and ρ_b is the bulk water density. To quantify the density fluctuations, we measured $P_v(N)$, the probability distribution for finding N water molecules in an observation volume v adjacent to the clay surface, using the indirect umbrella sampling (INDUS) method.[27,28] We chose a rectangular parallelepiped with dimensions of 15 Å × 15 Å × 3 Å placed near the surface as the observation volume (see Figure 1b). The exact z position of v was chosen to make the mean water density in v equal to ρ_b. The simulation box also contained a fixed wall of repulsive WCA particles (not shown) placed at the top of the box (far from v) to nucleate a vapor−liquid buffering interface.

Contact Angle. The simulation setup for contact angle measurements is shown in Figure 1c. The contact angle was determined by computing water density maps in the plane of the center of mass of the drop. The curve with a density equal to half of ρ_b was then fit to a circle, and the angle between the tangent to this circle at z_S = 7 Å and the horizontal axis was taken to be the contact angle. While the exact quantitative value of the contact angle depends on the choice of z_S, our qualitative findings do not.

Water Vapor Adsorption. The adsorption of water vapor at low RH corresponds the interaction of an isolated water molecule with the surface. To determine the corresponding adsorption free energy, $\Delta\mu_{ads}$, we computed $\mathcal{A}(z)$ using umbrella sampling, with the weighted histogram analysis method (WHAM)[34,35] being used to reconstruct $\mathcal{A}(z)$ from the biased trajectories.

RESULTS AND DISCUSSION

Hydrophobicity at Low and High RH. Using the various molecular measures of hydrophobicity described above, we studied talc, fluorotalc, and pyrophyllite surfaces at both saturation and low RH.

High RH. Theory[36−39] and simulations[27,40−43] have shown that the mean water density near a surface is not a good measure of the hydrophobicity of the surface. Instead, fluctuations away from the mean, particularly the rare fluctuations[27] indicating the cost of creating a cavity at the interface, are quantitatively correlated with the contact angle.[44] Patel et al.[27] have shown that hydrophobic surfaces display an enhanced probability of density depletion or a low-N fat tail in the $P_v(N)$ distribution, while $P_v(N)$ near hydrophilic surfaces is similar to that in bulk water. As shown in Figure 2a, $P_v(N)$ near all three clay surfaces displays a low-N fat tail, indicating that these surfaces are hydrophobic. A slight lifting of the fat tail from talc to fluorotalc and pyrophyllite suggests a corresponding marginal increase in hydrophobicity.

Another way to probe surface hydrophobicity is by simulating a sufficiently large water droplet on the surface and estimating the corresponding contact angle. Figure 2b shows the average shape of droplets on the clay surfaces. The curve corresponding to $\rho(r, z) = 0.5\rho_b$ is a circle in the rz plane, where r is the distance from the axis that passes through the center of mass of the droplet. The contact angles obtained from tangents drawn at z_S = 7 Å on the three surfaces are similar (talc, 96°; fluorotalc, 103°; pyrophyllite, 105°) and clearly indicate hydrophobic behavior.

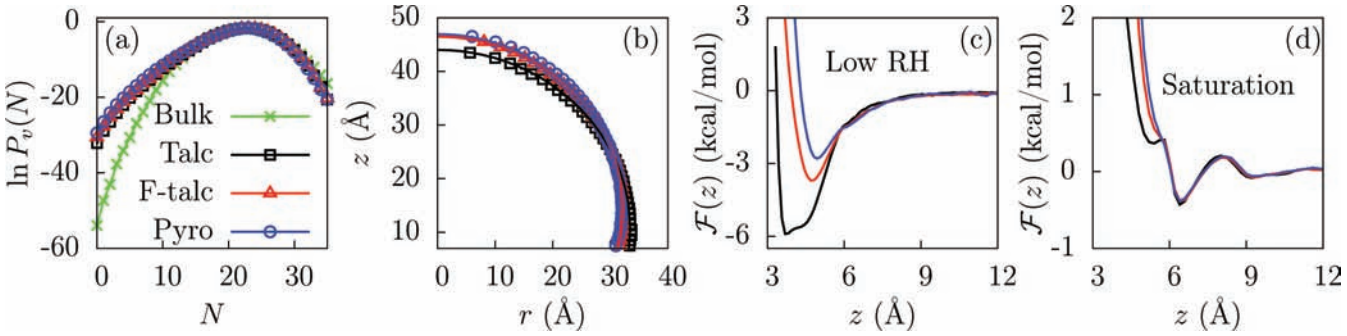

Figure 2. (a) $P_v(N)$, the probability of observing N water molecules in a probe volume v (15 Å × 15 Å × 3 Å), displays a low-N fat tail when v is near the surface of talc (black), fluorotalc (red), and pyrophyllite (blue), in comparison with that when v is in bulk water (green). (b) Water droplet profiles corresponding to $\rho(r, z) = 0.5\rho_b$ are shown for the clay surfaces. The contact angles for the surfaces are similar: 96° for talc, 103° for fluorotalc, and 105° for pyrophyllite (based on tangents drawn at z_S = 7 Å). (c) Potential of mean force, $\mathcal{F}(z)$, for the adsorption of an isolated water molecule (low RH) to the clay surfaces. The H atoms of the talc −OH groups are located at z = 2 Å and can participate in hydrogen bonds with water molecules. (d) $\mathcal{F}(z)$ at the clay−liquid water interface (saturation). To maximize hydrogen bonding with other waters, the binding site is no longer occupied.

Reliable experimental estimates of the contact angles for water droplets on both talc and pyrophyllite monocrystals are 80−85°.[25,26] The reported values for measurements on powders are usually smaller because of the presence of hydrophilic sites at the edges of finite clay particles.[45] To the best of our knowledge, no experimental contact angles have been reported for fluorotalc. For both talc and pyrophyllite, the contact angles obtained from our simulations (96° and 105°, respectively) are somewhat larger than the experimental estimates, suggesting that surfaces modeled with the CLAYFF model are too hydrophobic. Nevertheless, among various commonly used clay force fields,[46−48] we have found that the correspondence with experiments is closest for CLAYFF. A comparison of these force fields with experiments is provided in the Supporting Information.

Low RH. To investigate the wetting behavior of clay surfaces at low RH, we calculated $\mathcal{F}(z)$, the PMF for the adsorption of an isolated water molecule. $\mathcal{F}(z)$ displays a minimum near all the clay surfaces (see Figure 2c), corresponding to an adsorption (or binding) free energy, $\Delta\mu_{ads}$. For talc, $\Delta\mu_{ads} \approx -5.9$ kcal/mol, or $10k_BT$, consistent with the formation of a hydrogen bond between the water molecule and the hydroxyl group in talc. In fluorotalc, the hydroxyl group is replaced by fluorine, resulting in a reduction in $\Delta\mu_{ads}$ to −3.5 kcal/mol. The location of the minimum is also shifted outward by ∼1 Å, as the water is no longer strongly bound to the surface. Pyrophyllite, in which the hydroxyl group is parallel to the surface, has an even smaller value ($\Delta\mu_{ads} \approx -2.8$ kcal/mol), and the minimum is shifted out even more.

To compare our estimates of $\Delta\mu_{ads}$ from simulations to experimental data, we analyzed the data of Michot et al.[24] using a Langmuir model. This model assumes that there are no interactions between the adsorbed molecules and predicts a surface coverage, Θ, given by $\Theta = (P/P^*)/(1 + P/P^*)$, where P^* is the pressure at which half of the surface sites are occupied. P^* is related to $\Delta\mu_{ads}$ through

$$P^* = \frac{\sigma_{max} k_B T}{\delta} e^{\beta \Delta\mu_{ads}} \quad (1)$$

where $\sigma_{max} \approx 4.2$ nm^{-2} is the surface site density, $\delta \approx 1-2$ Å is the width of the surface layer (i.e., the width of the PMF well in Figure 2c), and $1/\beta = k_BT$ is the thermal energy.

In the very low RH limit, corresponding to adsorption of a single water molecule, we can safely assume that water molecules do not interact with each other. In this regime, $\Theta \approx P/P^*$, and the data in Figure 11 of ref 24 allowed us to obtain an experimental estimate of $P^* \approx 0.056P_{sat}$ for the talc surface. Here, P_{sat} = 30 mbar is the saturation pressure of water. Using this value of P^* in eq 1 gives an experimental estimate of $\Delta\mu_{ads} \approx -8$ kcal/mol.[49] This indicates that the adsorption is somewhat stronger than predicted from simulations using CLAYFF (−5.9 kcal/mol), consistent with the overestimate of the talc contact angle by CLAYFF.

If we further assume that the adsorbed water molecules do not interact with each other even at higher RH, the Langmuir model (with $P^* = 0.056P_{sat}$) predicts that $\Theta \approx 0.9$ at 50% RH. As water coverage on the talc surface can be large even at moderate RH, interactions between water molecules may be important, consistent with suggestions that clustering needs to be considered.[24,50] In contrast, for fluorotalc, the value of Θ at saturation estimated from $\Delta\mu_{ads}$ is very small (∼1.5%), in agreement with the hydrophobic adsorption behavior reported in Figure 10 of ref 24.

Thus, the clay surfaces simulated using the CLAYFF force field were more hydrophobic than the real clay surfaces used in experiments. However, the interesting dichotomy of talc surfaces was also observed in the simulations, and our findings are qualitatively consistent with the experiments at both low RH (strong adsorption for talc and not the other clays) and high RH (large contact angles for all of the clays).

Cohesion versus Adhesion. To investigate the disparate behavior of talc surfaces at low and high RH, we compared the $\mathcal{F}(z)$ curves for moving a water molecule away from the surfaces under these two sets of conditions. At saturation, the $\mathcal{F}(z)$ curves for the clay surfaces are similar (Figure 2d), consistent with the similar droplet contact angles on the three surfaces (Figure 2b). $\mathcal{F}(z)$ for fluorotalc is nearly identical to that for pyrophyllite, and that for talc features an additional local minimum at $z \approx 5$ Å corresponding to water molecules above the binding site. However, the $\mathcal{F}(z)$ curves at saturation (Figure 2d) are qualitatively different from those at low RH (Figure 2c). For all three clays, and especially so for talc, the depth of the minimum at saturation is smaller than that at low RH, suggesting a weakening of adhesive interactions at saturation. The average number of hydrogen bonds donated by the surface hydroxyl groups of talc is ΘN_{HB}, where N_{HB} is the average number of hydrogen bonds donated per occupied site. At low RH, $N_{HB} \approx 0.83$, while at

saturation it drops to only 0.02 as a result of the hydrogen bonding to other water molecules.

To explore the competition between adhesive and cohesive interactions in talc, we compared $\mathcal{F}(z)$ curve for an individually adsorbed water molecule with those for water in a dimer and water at saturation. As shown in Figure 3, $\mathcal{F}(z)$ for the dimer displays two minima. The minimum corresponding to the molecule inside the cavity is shifted to slightly larger z relative to the minimum in $\mathcal{F}(z)$ for a single water molecule. In addition, the depth of the minimum is smaller and comparable to that for a single water molecule on the more hydrophobic fluorotalc surface (Figure 2c). In other words, the presence of the second water molecule weakens the adhesive surface−water interactions, which have to compete with the cohesive interactions between the water molecules. As the dimer is less tightly bound to the surface than a single molecule, it is easier for the water to escape the cavity in the presence of a second molecule. The dimer is in fact more mobile on the talc surface than isolated water molecules (not shown), confirming that the interaction of the surface with the dimer is weaker than with individual molecules. Finally, at saturation, cohesive interactions prevail, and water no longer occupies the binding site cavity, as evidenced by the lack of a minimum in $\mathcal{F}(z)$ for 3 Å < z < 5 Å.

Modified Talc Surfaces. While the hydrogen bonding between binding sites on the talc surface and water leads to an interesting transition from hydrophilic at low RH to hydrophobic at high RH, the binding sites interact weakly with water in fluorotalc and pyrophyllite, which display hydrophobic behavior for all RH. To investigate the effect of the binding strength on the hydrophobicity of the surface, following Giovambattista et al.,[51] we constructed a series of modified talc surfaces. The only force field parameters that were changed were the charges on the oxygen (from $q_O = -0.95$ to $q_O - \delta q$) and the hydrogen (from $q_H = 0.425$ to $q_H + \delta q$) of the hydroxyl group. We studied modified talc surfaces with δq ranging from −0.425, which corresponds to a nonpolar binding site similar to that in fluorotalc, to +0.6, which corresponds to an ion pair. By definition, $\delta q = 0$ corresponds to the talc surface.

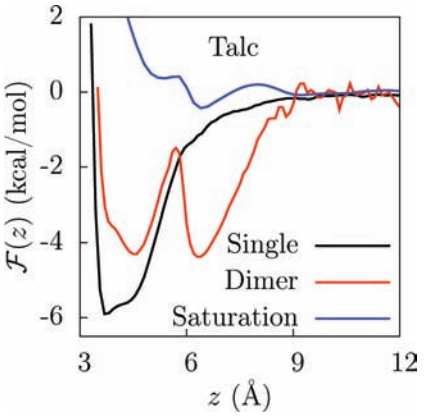

Figure 3. $\mathcal{F}(z)$ for adsorption a single water molecule on the talc surface (black) compared with those for a molecule in a dimer (red) and a molecule at saturation (blue).

In Figure 4a, we show $\mathcal{F}(z)$ for an isolated water molecule on each of the modified talc surfaces. As the polarity of the −OH bond increases, the magnitude of $\Delta\mu_{ads}$ also increases, providing us with surfaces that display a wide range of binding strengths. $\mathcal{F}(z)$ at saturation for these surfaces (shown in Figure 4b) is particularly interesting. For weakly adhesive surfaces ($-0.425 \leq \delta q < 0.1$), there is only one stable basin at $z \approx 6.5$ Å, corresponding to molecules outside the binding site cavity. For stronger adhesion (larger δq), a second basin develops at $z \approx 3.5$ Å and is separated from the first basin by a barrier.

Figure 4c shows the depth of this minimum relative to the bulk, $\Delta\mu_{site}$, as a function of $\Delta\mu_{ads}$. As the surface becomes more adhesive, more waters occupy the binding site, and the depth of this minimum increases. When adhesive interactions are large enough to overcome cohesive interactions, that is, when $-\Delta\mu_{ads}$ becomes larger than the chemical potential at saturation, $-\mu_{sat}$ (for $\delta q \approx 0.4$), every binding site is occupied by a water molecule, resulting in a plateau in $\Delta\mu_{site}$. The average number of hydrogen bonds donated by surface hydroxyl groups also behaves as $\Delta\mu_{site}$; its dependence on $\Delta\mu_{ads}$ is provided in the Supporting Information.

However, the height of the barrier to escape the cavity, $\Delta\mu_{barrier}$ (also shown in Figure 4c), continues to increase approximately linearly with the binding strength. Thus, for surfaces with strong binding, $\Delta\mu_{barrier}$ is large, and the exchange of molecules between the cavities and the liquid is expected to be very slow, with possible consequences for the extent of stick/slip at such surfaces in the presence of a hydrodynamic flow.

Tuning Cohesion/Adhesion via RH/$\Delta\mu_{ads}$. Collectively, our results paint a comprehensive picture of how the experimentally measurable quantities (the surface coverage Θ and the contact angle θ) respond to changes in RH (or water chemical potential) and the strength of the adhesive surface−water interactions.

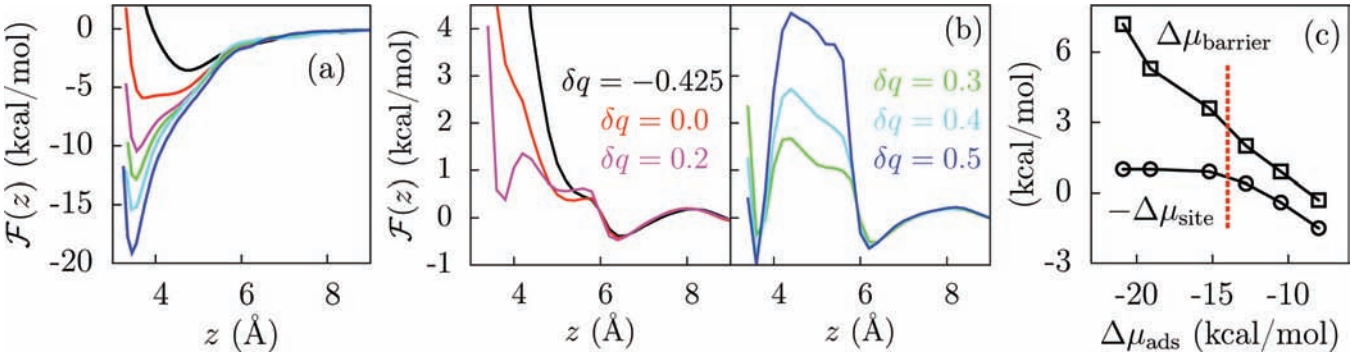

Figure 4. (a) $\mathcal{F}(z)$ curves for a single water molecule on various talc surfaces modified to span a range of $\Delta\mu_{ads}$ values. (b) The corresponding $\mathcal{F}(z)$ curves at saturation. (c) Relative stability of water in the binding site relative to that in bulk, $-\Delta\mu_{site}$, and the barrier to escape from the binding site, $\Delta\mu_{barrier}$, as functions of the binding strength, $\Delta\mu_{ads}$. The dashed vertical line corresponds to μ_{sat}, the chemical potential at saturation.

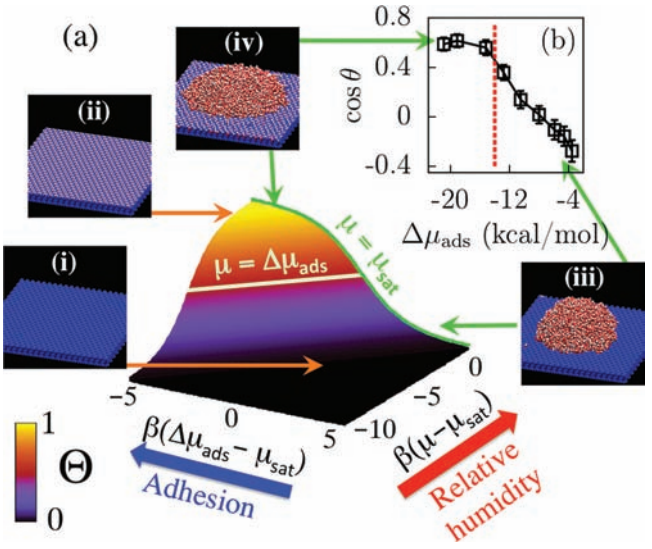

Figure 5. (a) Schematic showing the surface coverage, Θ, over a wide range of relative humidities (RH = $P/P_{sat} \approx \exp[\beta(\mu - \mu_{sat})]$) and adhesive interaction strengths ($\Delta\mu_{ads}$). (b) Effect of $\Delta\mu_{ads}$ on the surface hydrophobicity, as quantified by cos θ, where θ is the contact angle. The dashed vertical line corresponds to μ_{sat}. Snapshots indicating typical configurations of water molecules (red and white) on modified talc surfaces (blue) are also shown. As the adhesive interactions ($\Delta\mu_{ads}$) overcome the cohesive interactions (μ), there is a transition from a dry surface [snapshots (i) and (iii)] to one covered with a monolayer of water [snapshots (ii) and (iv)].

The surface coverage Θ is defined as the fraction of binding sites occupied by water molecules, and its dependence on RH and $\Delta\mu_{ads}$ is shown schematically in Figure 5a.

At low RH ($\equiv P/P_{sat}$), the competition between the adhesive interactions and the entropy of being in the vapor determines the surface coverage, Θ. At very low RH, there are no interactions between adsorbed water molecules, and Θ can be approximated as

$$\Theta \approx \frac{P}{P^*} = 0.1\left(\frac{P}{P_{sat}}\right)e^{-\beta\Delta\mu_{ads} - 8.3} \qquad (2)$$

where the second part of the equation was obtained by substituting for P^* using eq 1 and using appropriate values of the constants that depend on the surface geometry (σ_{max} and δ) and the thermodynamic conditions (T and P_{sat}).

For surfaces with small adhesive interactions (i.e., $-\Delta\mu_{ads} < 5$ kcal/mol or $-\beta\Delta\mu_{ads} < 8.3$), the coverage remains small ($\Theta < 0.1$) even at saturation [snapshot (i) in Figure 5]. Thus, no appreciable interactions between water molecules are expected over the entire range of RH values. Both pyrophyllite and fluorotalc fall in this regime.

Since Θ increases exponentially with $\beta\Delta\mu_{ads}$, for values of $-\Delta\mu_{ads} > 5$ kcal/mol, there can be substantial coverage even at modest RH [snapshot (ii) in Figure 5]. Equation 2 is then valid only for small RH values, for which the predicted Θ values are small. Talc lies in this regime.

For larger RH values, there are appreciable interactions between the water molecules, and it is the competition between adhesive and cohesive interactions that determines surface properties. For surfaces such as talc, for which $-\Delta\mu_{ads} < -\mu_{sat}$, cohesion prevails at saturation, and the adsorbed waters bead up into a droplet, while the rest of the binding sites on the surface are devoid of water [snapshot (iii) in Figure 5]. Thus, the interesting crossover from hydrophobic to hydrophilic behavior in talc is a result of its adhesive interactions being strong enough to overcome the vapor-phase entropy at low RH but not strong enough to overcome cohesive interactions at saturation. In this regime, with increasing polarity of the binding site, the surface gradually shifts from hydrophobic to hydrophilic and cos θ increases approximately linearly, as shown in Figure 5b.

Finally, for surfaces with even larger values of $-\Delta\mu_{ads}$ that are greater than $-\mu_{sat}$, adhesion dominates. Surprisingly, water does not fully wet the surface at saturation. Instead, all of the binding sites are occupied by water molecules and only this first layer of water wets the surface. This water is strongly bound to the surface, and the microstructure of the surface dictates the relative positions of the waters. In the present case, the arrangement of waters on the surface is not commensurate with the hydrogen-bonding network of water, so water beads up on the monolayer [snapshot (iv) in Figure 5]. For the modified talc surfaces with $-\Delta\mu_{ads} > -\mu_{sat}$, the surface has a strongly adsorbed water monolayer with a droplet on it that makes a contact angle of ~50°.

Concluding Remarks: Surface Details Matter. Similar behavior was reported by Ohler and Langel[52] for titanium dioxide surfaces, with droplet contact angles of 32−34° on top of roughly two monolayers of water, and by Wang et al.,[53] who studied model polar surfaces with hexagonal charge patterns and observed a water droplet atop an ice-like water monolayer. However, other simulation studies investigating the effects of surface polarity on hydrophobicity[54,55] did not observe a plateau with nonzero contact angle at large polarities, as seen in our results (Figure 5b). Our modified talc surfaces are different from the ones in these previous studies in that the variation in polarity was achieved by changing the charges on atoms in recessed binding sites while keeping the remaining surface atoms unchanged. In contrast, in ref 54, the surface was modified by changing dipoles that protrude from the surface while leaving the remaining surface atoms unchanged, whereas in ref 55, the charges on all atoms in the top two layers of a face-centered cubic (fcc) crystal (111 facet) were changed to tune the polarity. Thus, our results indicate that the microstructure of the surface is important in determining the effect of polarity on its wetting properties.

In contrast to the wetting properties of the model fcc surfaces used in ref 55, experimental measurements indicate that the fcc crystals of platinum, palladium, and gold are hydrophobic. Kimmel et al.[56,57] observed a hydrophobic water monolayer on both Pt(111) and Pd(111) crystals. Similarly, water has been shown to bead up on Au surfaces[58] with a contact angle of 100°, and Au surfaces have also been shown to adsorb and facilitate the unfolding of proteins;[59] such behavior is typically associated with hydrophobic surfaces.[44] We speculate that the hydrophobicity of these metal surfaces arises from the presence of a monolayer of water that binds strongly to the surface in a geometry that inhibits hydrogen bonding to the subsequent liquid water molecules.

Our results also have implications for the wetting properties of nanoporous silicates such as hydrophobic zeolites[60−62] and metal−organic frameworks.[63] These hydrophobic pores are thought to be devoid of water under ambient conditions, with water intrusion into the pores occurring only at sufficiently high water pressures. Our results suggest that in the presence of strong binding sites, these nanoporous materials may contain strongly adsorbed water molecules even at lower pressures. If the resulting water-covered surface is hydrophobic, no further filling of the

pores (analogous to wetting for planar surfaces) would be observed at ambient pressures, and intrusion would occur only at higher pressures.

■ ASSOCIATED CONTENT

Supporting Information. Unit cells for the different clays, comparison of force fields, and numbers of hydrogen bonds donated by modified talc surface hydroxyl groups to interfacial water molecules. This material is available free of charge via the Internet at http://pubs.acs.org.

■ AUTHOR INFORMATION

Corresponding Author
benjamin.rotenberg@upmc.fr

■ ACKNOWLEDGMENT

The authors thank Virginie Marry, Patrick Varilly, Mark Davis, Shekhar Garde, and Adam Willard for helpful discussions. B.R. is grateful to the University of California, Berkeley, for its hospitality. A.J.P. was supported by NIH Grant R01-GM078102-04. D.C. was supported by the Director, Office of Science, Office of Basic Energy Sciences, Materials Sciences and Engineering Division and Chemical Sciences, Geosciences, and Biosciences Division, of the U.S. Department of Energy under Contract DE-AC02-05CH11231.

■ REFERENCES

(1) Bridgeman, C.; Buckingham, A.; Skipper, N.; Payne, M. *Mol. Phys.* **1996**, *89*, 879–888.
(2) Churakov, S. V. *Geochim. Cosmochim. Acta* **2007**, *71*, 1130–1144.
(3) Cygan, R. T.; Liang, J.-J.; Kalinichev, A. G. *J. Phys. Chem. B* **2004**, *108*, 1255–1266.
(4) Cygan, R. T.; Greathouse, J. A.; Heinz, H.; Kalinichev, A. G. *J. Mater. Chem.* **2009**, *19*, 2470.
(5) Delville, A. *Langmuir* **1991**, *7*, 547–555.
(6) Marry, V.; Turq, P. *J. Phys. Chem. B* **2003**, *107*, 1832–1839.
(7) Boek, E.; Coveney, P.; Skipper, N. *J. Am. Chem. Soc.* **1995**, *117*, 12608–12617.
(8) Sposito, G.; Skipper, N.; Sutton, R.; Park, S.; Soper, A.; Greathouse, J. *Proc. Natl. Acad. Sci. U.S.A.* **1999**, *96*, 3358–3364.
(9) Delville, A. *Langmuir* **1992**, *8*, 1796–1805.
(10) Young, D.; Smith, D. *J. Phys. Chem. B* **2000**, *104*, 9163–9170.
(11) Hensen, E.; Smit, B. *J. Phys. Chem. B* **2002**, *106*, 12664–12667.
(12) Tambach, T.; Bolhuis, P.; Smit, B. *Angew. Chem., Int. Ed.* **2004**, *43*, 2650–2652.
(13) Teppen, B. J.; Miller, D. M. *Soil Sci. Soc. Am. J.* **2006**, *70*, 31–40.
(14) Rotenberg, B.; Marry, V.; Vuilleumier, R.; Malikova, N.; Simon, C.; Turq, P. *Geochim. Cosmochim. Acta* **2007**, *71*, 5089–5101.
(15) Rotenberg, B.; Morel, J.; Marry, V.; Turq, P.; Morel-Desrosiers, N. *Geochim. Cosmochim. Acta* **2009**, *73*, 4034–4044.
(16) Wang, J.; Kalinichev, A. G.; Kirkpatrick, R.; Cygan, R. *J. Phys. Chem. B* **2005**, *109*, 15893–15905.
(17) Marry, V.; Rotenberg, B.; Turq, P. *Phys. Chem. Chem. Phys.* **2008**, *10*, 4802–4813.
(18) Wang, J.; Kalinichev, A. G.; Kirkpatrick, R. *Earth Planet. Sci. Lett.* **2004**, *222*, 517–527.
(19) Wang, J.; Kalinichev, A. G.; Kirkpatrick, R. J. *J. Phys. Chem. B* **2005**, *109*, 14308–14313.
(20) Wang, J.; Kalinichev, A. G.; Kirkpatrick, R. *Geochim. Cosmochim. Acta* **2006**, *70*, 562–582.
(21) Wang, J.; Kalinichev, A. G.; Kirkpatrick, R. J. *J. Phys. Chem. C* **2009**, *113*, 11077–11085.
(22) Tunega, D.; Benco, L.; Haberhauer, G.; Gerzabek, M. H.; Lischka, H. *J. Phys. Chem. B* **2002**, *106*, 11515–11525.
(23) Tunega, D.; Gerzabek, M. H.; Lischka, H. *J. Phys. Chem. B* **2004**, *108*, 5930–5936.
(24) Michot, L. J.; Villieras, F.; Francois, M.; Yvon, J.; Le Dred, R.; Cases, J. M. *Langmuir* **1994**, *10*, 3765–3773.
(25) Giese, R.; Costanzo, P.; Oss, C. *Phys. Chem. Miner.* **1991**, *17*, 611–616.
(26) Van Oss, C. J.; Giese, R. F. *Clays Clay Miner.* **1995**, *43*, 474–477.
(27) Patel, A. J.; Varilly, P.; Chandler, D. *J. Phys. Chem. B* **2010**, *114*, 1632–1637.
(28) Patel, A. J.; Varilly, P.; Chandler, D.; Garde, S. *J. Stat. Phys.* [Online early access]. DOI: 10.1007/s10955-011-0269-9. Published Online: Aug 10, 2011.
(29) Berendsen, H. J. C.; Grigera, J. R.; Straatsma, T. P. *J. Phys. Chem.* **1987**, *91*, 6269–6271.
(30) Dang, L. X. *Chem. Phys. Lett.* **1992**, *200*, 21–25.
(31) LAMMPS Molecular Dynamics Simulator. http://lammps.sandia.gov (accessed Sept 18, 2011).
(32) Martyna, G.; Klein, M.; Tuckerman, M. *J. Chem. Phys.* **1992**, *97*, 2635–2643.
(33) Ryckaert, J.-P.; Ciccotti, G.; Berendsen, H. *J. Comput. Phys.* **1977**, *23*, 327–341.
(34) Kumar, S.; Rosenberg, J. M.; Bouzida, D.; Swendsen, R. H.; Kollman, P. A. *J. Comput. Chem.* **1995**, *16*, 1339–1350.
(35) Roux, B. *Comput. Phys. Commun.* **1995**, *91*, 275–282.
(36) Lum, K.; Chandler, D.; Weeks, J. D. *J. Phys. Chem. B* **1999**, *103*, 4570–4577.
(37) Chandler, D. *Nature* **2005**, *437*, 640–647.
(38) Berne, B. J.; Weeks, J. D.; Zhou, R. *Annu. Rev. Phys. Chem.* **2009**, *60*, 85–103.
(39) Varilly, P.; Patel, A. J.; Chandler, D. *J. Chem. Phys.* **2011**, *134*, No. 074109.
(40) Mittal, J.; Hummer, G. *Proc. Natl. Acad. Sci. U.S.A.* **2008**, *105*, 20130–20135.
(41) Sarupria, S.; Garde, S. *Phys. Rev. Lett.* **2009**, *103*, No. 037803.
(42) Godawat, R.; Jamadagni, S. N.; Garde, S. *Proc. Natl. Acad. Sci. U.S.A.* **2009**, *106*, 15119–15124.
(43) Acharya, H.; Vembanur, S.; Jamadagni, S. N.; Garde, S. *Faraday Discuss.* **2010**, *146*, 353–365.
(44) Patel, A. J.; Varilly, P.; Jamadagni, S. N.; Acharya, H.; Garde, S.; Chandler, D. *Proc. Natl. Acad. Sci. U.S.A.* **2011**, *108*, 17678–17683.
(45) Douillard, J. *J. Colloid Interface Sci.* **2002**, *255*, 341–351.
(46) Skipper, N.; Refson, K.; McConnell, J. *Clay Miner.* **1989**, *24*, 411–425.
(47) Smith, D. *Langmuir* **1998**, *14*, 5959–5967.
(48) Heinz, H.; Koerner, H.; Anderson, K. L.; Vaia, R. A.; Farmer, B. L. *Chem. Mater.* **2005**, *17*, 5658–5669.
(49) Since the number of hydrophilic binding sites on clay edges is much smaller than that on the talc surface, we neglected the edge sites to obtain this estimate.
(50) Carvalho, A.; Ramalho, J.; Villieras, F. *Appl. Surf. Sci.* **2007**, *253*, 5628–5632.
(51) Giovambattista, N.; Debenedetti, P. G.; Rossky, P. J. *J. Phys. Chem. B* **2007**, *111*, 9581–9587.
(52) Ohler, B.; Langel, W. *J. Phys. Chem. C* **2009**, *113*, 10189–10197.
(53) Wang, C.; Lu, H.; Wang, Z.; Xiu, P.; Zhou, B.; Zuo, G.; Wan, R.; Hu, J.; Fang, H. *Phys. Rev. Lett.* **2009**, *103*, No. 137801.
(54) Giovambattista, N.; Debenedetti, P. G.; Rossky, P. J. *Proc. Natl. Acad. Sci. U.S.A.* **2009**, *106*, 15181–15185.
(55) Surblys, D.; Yamaguchi, Y.; Kuroda, K.; Nakajima, T.; Fujimura, H. *J. Chem. Phys.* **2011**, *135*, No. 014703.
(56) Kimmel, G. A.; Petrik, N. G.; Dohnalek, Z.; Kay, B. D. *Phys. Rev. Lett.* **2005**, *95*, No. 166102.
(57) Kimmel, G. A.; Petrik, N. G.; Dohnalek, Z.; Kay, B. D. *J. Chem. Phys.* **2007**, *126*, No. 114702.
(58) Anand, G.; Sharma, S.; Dutta, A. K.; Kumar, S. K.; Belfort, G. *Langmuir* **2010**, *26*, 10803–10811.

(59) Anand, G.; Zhang, F.; Linhardt, R. J.; Belfort, G. *Langmuir* **2011**, *27*, 1830–1836.
(60) Cailliez, F.; Trzpit, M.; Soulard, M.; Demachy, I.; Boutin, A.; Patarin, J.; Fuchs, A. H. *Phys. Chem. Chem. Phys.* **2008**, *10*, 4817.
(61) Cailliez, F.; Stirnemann, G.; Boutin, A.; Demachy, I.; Fuchs, A. H. *J. Phys. Chem. C* **2008**, *112*, 10435–10445.
(62) Moliner, M.; Roman-Leshkov, Y.; Davis, M. E. *Proc. Natl. Acad. Sci. U.S.A.* **2010**, *107*, 6164.
(63) Paranthaman, S.; Coudert, F.-X.; Fuchs, A. H. *Phys. Chem. Chem. Phys.* **2010**, *12*, 8123.